Yamina BENHADDA[1], Fatima Zohra MEDJAOUI[1], Abderrahim MOKHFI[2], Azzedine HAMID[3], V. BLEY[4]

USTO-MB University, Oran, Algeria(1), ENP, Oran, Algeria (2) , Center Nour Bachir, El Bayadh, Algeria (3), Toulouse University III Paul Sabatier, France (4)

doi:10.15199/48.2024.08.27

Cooling Optimization of Integrated Planar Spiral Inductor with Heat Sink

Abstract. *This paper presents a comprehensive cooling optimization of an integrated planar spiral inductor with heat sink through a numerical simulation approach. The study utilizes COMSOL 6.0 software, employing the finite element method to perform the simulations. The investigation focuses on evaluating the temperature distribution in the integrated inductor under different conditions. Without the heat sink, the maximum temperature observed in the integrated inductor is 66.1°C. However, with the integration of a heat sink featuring diamond fins, the temperature distribution improves significantly, resulting in a maximum temperature of 31.9°C.The simulation also examines the viscosity distribution, revealing the efficient propagation of air towards the heat sink, contributing to the cooling process. However, it is worth noting that there is a substantial pressure build-up in the air gap between the upper part of the heat sink and the ceramic plaque, which can impact the overall cooling effectiveness. Moreover, the study investigates the influence of different fin shapes on temperature distribution. The rectangular fins prove to be particularly effective in removing heat from the integrated inductor, leading to a maximum temperature of 31.7°C. On the other hand, the square fins demonstrate efficient heat dissipation, resulting in a maximum temperature of 33.8°C.*

Streszczenie. *W artykule przedstawiono kompleksową optymalizację chłodzenia zintegrowanej płaskiej cewki spiralnej z radiatorem za pomocą symulacji numerycznej. W badaniach wykorzystano oprogramowanie COMSOL 6.0, w którym do przeprowadzenia symulacji wykorzystano metodę elementów skończonych. Badania skupiają się na ocenie rozkładu temperatury w zintegrowanej cewce indukcyjnej w różnych warunkach. Bez radiatora maksymalna temperatura obserwowana w zintegrowanej cewce wynosi 66,1°C. Jednakże dzięki integracji radiatora z żeberkami diamentowymi rozkład temperatury znacznie się poprawia, osiągając maksymalną temperaturę 31,9°C. Symulacja bada również rozkład lepkości, ujawniając efektywną propagację powietrza w kierunku radiatora, przyczyniając się do procesu chłodzenia. Warto jednak zauważyć, że w szczelinie powietrznej pomiędzy górną częścią radiatora a płytką ceramiczną następuje znaczny wzrost ciśnienia, co może mieć wpływ na ogólną skuteczność chłodzenia. W pracy zbadano także wpływ różnych kształtów żeberek na rozkład temperatury. Prostokątne żebra okazują się szczególnie skuteczne w usuwaniu ciepła ze zintegrowanego induktora, co pozwala uzyskać maksymalną temperaturę 31,7°C. Z drugiej strony kwadratowe lamele skutecznie odprowadzają ciepło, co daje maksymalną temperaturę 33,8°C. (**Optymalizacja chłodzenia zintegrowanego płaskiego spiralnego induktora z radiatorem**)*

Keywords: thermal, cooling, inductor, heat sink.
Słowa kluczowe: termo–chłodzenie, cewka indukcyjna, radiator.

Introduction

Inductors play a crucial role in switching power converters as they store electrical energy [1, 2]. However, when operating in switching power converters, these inductors can experience increased power losses due to the effect of current flow through the windings on the magnetic core's reversal [3]. These losses are converted to heat, leading to self-heating and thermal coupling between the inductor's core and windings, causing their temperature to rise above the ambient temperature [4-9]. To ensure the reliability and efficiency of power converters, it is essential to address the thermal challenges associated with inductor operation. In this paper, the focus is directed towards the optimization of cooling mechanisms for an integrated planar spiral inductor featuring a heat sink. The investigation unfolds through the employment of advanced numerical simulations conducted using Comsol 6.0 and the finite element method. This paper introduces the topography of planar square integrated inductors. The geometry of the integrated inductor coupled with a heat sink is meticulously presented. Additionally, the paper explores various configurations of heat sinks, including those adorned with diamond fins, rectangular fins, and square fins, each showcasing distinct heat dissipation properties. The mesh structure employed in the integrated inductor with the heat sink is detailed. The mathematical foundation for fluid dynamics is laid out through the presentation of the Navier-Stokes equations, serving as the cornerstone for the subsequent numerical simulations and analyses.

Structure of integrated inductor

Figure 1 shows the planar square integrated inductor topography. The integrated inductor is composed of a micro coil and a substrate. It features a planar spiral inductor with a new structure of an underpass to achieve high inductance, high quality factor, and minimum losses in the winding and magnetic core. The design aims to optimize the performance of the inductor for various electronic applications.

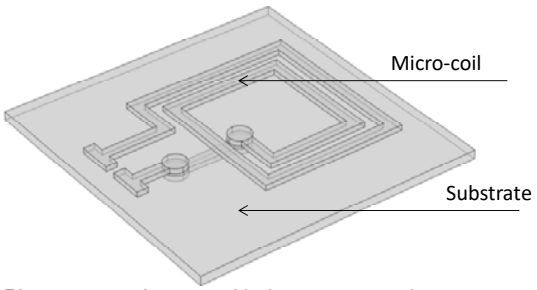

Fig.1. Planar square integrated inductor topography

Figure 2 illustrates the winding of the integrated inductor.

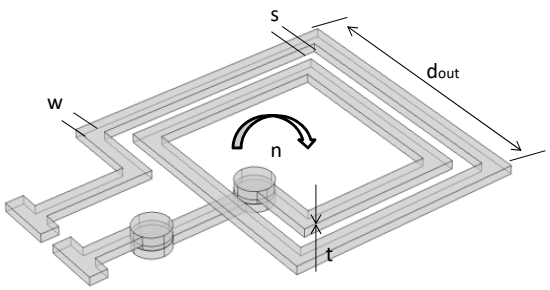

Fig.2. Winding of integrated inductor

Table 1 provides essential information about the integrated inductor's key parameters, offering valuable insights into its design and performance.

Table 1. Design results of the integrated inductor

Parameter	Value
Inductance, L (H)	$1.13\ 10^{-6}$
Output diameter, d_{out} (m)	$750\ 10^{-6}$
Number of turns, n	2
Thickness of the conductor, t (m)	$20\ 10^{-6}$
Width of the conductor, w (m)	$10\ 10^{-6}$
Spacing between conductor, s (m)	$10\ 10^{-6}$

Figure 3 illustrates the geometry of the integrated inductor with a heat sink. The micro-coil, responsible for inducing the magnetic field, is fabricated using copper, a highly conductive material suitable for this purpose. The substrate, on the other hand, is composed of kapton, chosen for its electrical insulation properties and flexibility.
In this design, the micro-coil is surrounded by air, which allows for effective cooling and dissipation of heat generated during operation. To further enhance thermal management, a heat sink made of aluminum is incorporated into the structure. The heat sink helps dissipate excess heat, preventing overheating and ensuring optimal performance and reliability of the integrated inductor.
To provide electrical isolation between the heat sink and the substrate, a ceramic plaque is used. This ceramic layer acts as an insulating barrier, preventing any unwanted electrical coupling between the components.

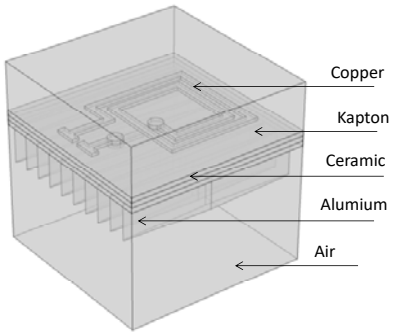

Fig.3. Geometry of integrated inductor with heat sink

Figure 4 displays the geometry of a heat sink with diamond fins. The innovative design features fins arranged in a diamond pattern, creating an efficient heat dissipation structure. The diamond fins allow for increased surface area and enhanced airflow, facilitating the transfer of heat away from the integrated components.

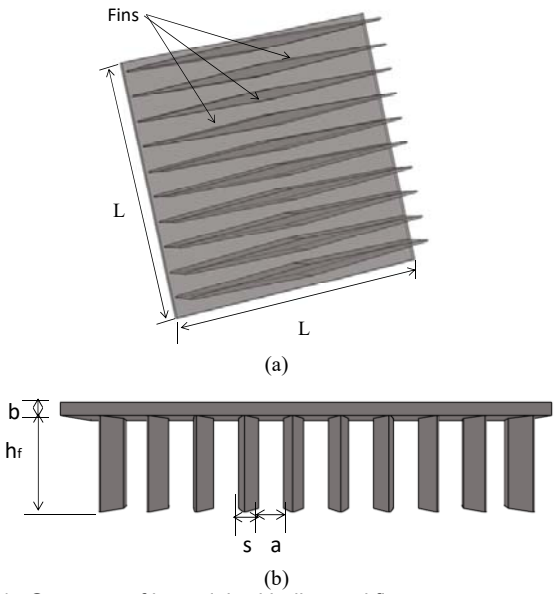

Fig. 4. Geometry of heat sink with diamond fins

Table 2 present a dimensions of heat sink.

Table 2. Dimensions of heat sink

Specifications	**Value (μm)**
Length of base, L	10200
Thickness of fins, s	400
Width between two fins, a	500
Height of fins, h_f	1000
Base thickness, b	275
Number of fins, N_f	10

Figure 5 illustrates the geometry of a heat sink with rectangular fins. In this design, the fins are arranged in a rectangular pattern, providing an effective surface area for heat dissipation.

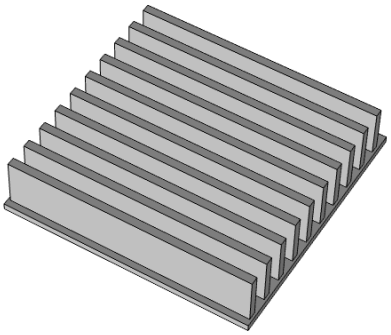

Fig.5. Geometry of heat sink with rectangular fins

Figure 6 displays the geometry of a heat sink with square fins.

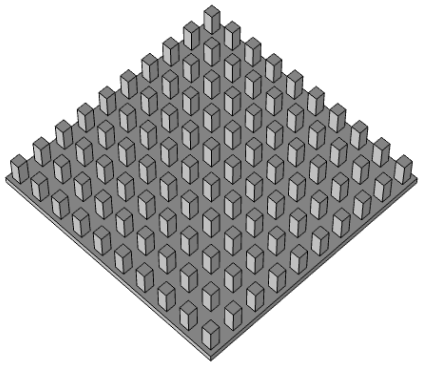

Fig.6. Geometry of heat sink with square fins

Numerical simulation

Numerical simulation was employed using COMSOL 6.0 based on the finite element method to analyze and model the behavior of the integrated inductor with a heat sink. Figure 7 presents the mesh of the integrated inductor with the heat sink. The mesh is a discretized representation of the computational domain, where the complex geometry of the inductor and heat sink is broken down into smaller, interconnected elements.

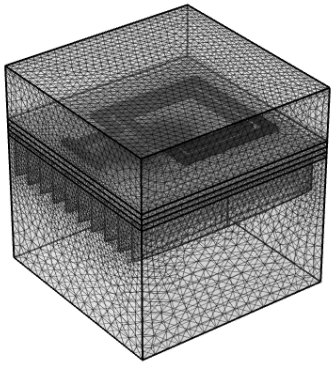

Fig.7. Mesh of integrated inductor with heat sink

The Navier-Stokes equations, which describe the momentum and energy for a moving fluid, are expressed by the following formula:

(1) $$\frac{\partial \rho_{air}}{\partial t} + \nabla \rho_{air} v = 0$$

(2) $$\rho_{air}\left[\frac{\partial v}{\partial t} + v.\nabla v\right] = -\nabla p + \mu_{air}\nabla^2 v$$

The heat transfer equation, which models the thermal energy transfer through the coil and the heat sink is given by the following formula:

(3) $$\rho_i Cp_i\left[\frac{\partial T}{\partial t} + v_{i=air}.\nabla T\right] = k_i \nabla^2 T + Q$$

Table 3 describe Electrical properties of components.

Table 3. Electrical properties of different components

Properties	Air	Copper	Kapton
Density (kg m^{-3})	1.225	8700	900
Viscosity (Pa s)	1.814×10^{-5}	-	-
Thermal conductivity (W m^{-1} K^{-1})	0.0257	400	0.7915
Heat capacity (J kg^{-1} K^{-1})	1005.4	385	751.67
Electrical resistivity (Ω m)	1.3×10^{16}	1.75×10^{-8}	15×10^{-2}
Relative permittivity	1.0000	1.0000	3.9000
Relative permeability	1.0000	1.0000	1.0000
Thermal expansion (10^{-3} K^{-1})	3.4300	-	-

Figure 8 presents the temperature distribution in the integrated inductor without a heat sink. The maximum temperature observed in the integrated inductor reaches 66.1°C. This temperature distribution indicates the heat generated during the operation of the inductor and highlights the need for efficient cooling solutions to maintain the temperature within a safe operating range.
Understanding the temperature distribution in the integrated inductor without a heat sink is essential for designing effective thermal management strategies. The findings from this simulation will aid in the optimization of cooling solutions, ensuring the reliability and performance of the integrated inductor and the overall power converter system.

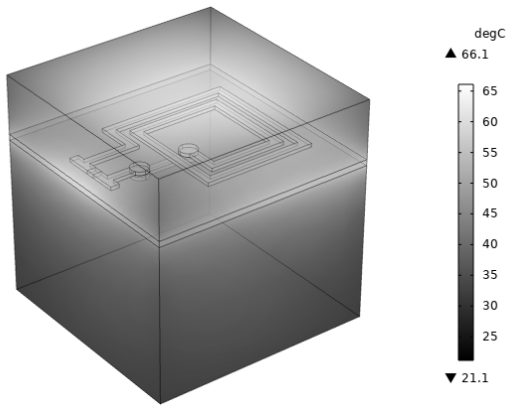

Fig.8. Temperature distribution in inductor without heat sink

Figure 9 presents the temperature distribution in integrated inductor with heat sink diamond fins. The heat sink's diamond fins effectively dissipate heat, resulting in a maximum temperature of 31.9 °C.

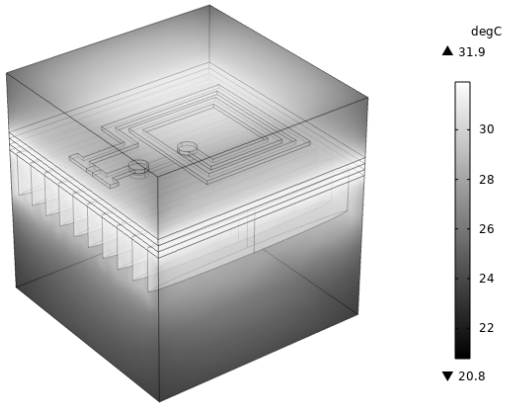

Fig.9. Temperature distribution in inductor with heat sink diamond fins

Figure 10 displays the viscosity distribution in the integrated inductor with heat sink diamond fins. The viscosity distribution demonstrates the propagation of air towards the heat sink. This directional flow is essential for efficient cooling, as air carries away the heat generated by the integrated inductor and transports it towards the heat sink. As the air moves through the inductor, it absorbs heat, subsequently lowering the temperature of the electronic components.

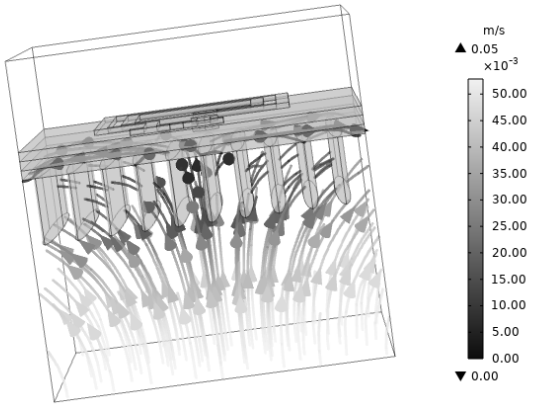

Fig. 10. Viscosity distribution in inductor with heat sink diamond fins

Figure 11 presents the pressure distribution in the integrated inductor with heat sink diamond fins. This pressure in the air is crucial as it plays a role in ensuring efficient thermal contact and conduction between the heat sink and the ceramic material.

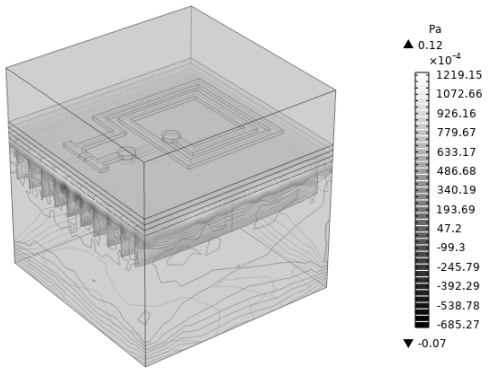

Fig. 11. Pressure distribution in inductor with heat sink diamond fins

Figure 12 presents the temperature distribution in integrated inductor with heat sink rectangular fins. The rectangular fins effectively remove heat from the integrated

inductor, resulting in a maximum temperature of 31.7°C. This indicates that the heat sink's design with rectangular fins effectively cools the integrated inductor, maintaining its temperature within a safe operating range and ensuring reliable performance.

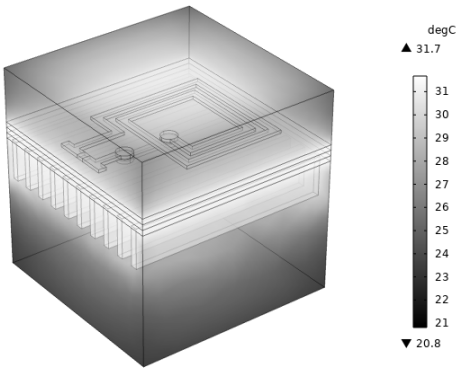

Fig. 12. Temperature distribution in inductor with heat sink rectangular fin

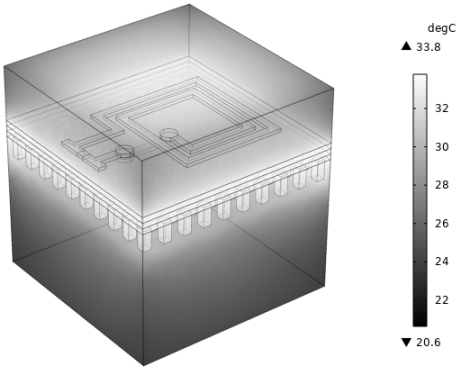

Fig/ 13. Temperature distribution in integrated inductor with heat sink square fins

Figure 13 depicts the temperature distribution in integrated inductor with heat sink square fins. Where the integrated inductor is equipped with heat sink square fins, the temperature distribution demonstrates efficient heat dissipation. The square fins effectively dissipate heat from the integrated inductor, resulting in a maximum temperature of 33.8°C.

Conclusion

This paper presents a cooling optimization of an integrated planar spiral inductor with heat sink, employing a numerical simulation approach. Utilizing COMSOL 6.0 software and the finite element method, the study investigates the thermal behavior of the integrated inductor under different cooling configurations. Without the heat sink, the maximum temperature observed in the integrated inductor reaches 66.1°C. With the integration of a heat sink featuring diamond fins, the temperature distribution improves considerably, resulting in a maximum temperature of 31.9°C. The analysis also reveals the efficient propagation of air towards the heat sink, as shown by the viscosity distribution. However, a notable finding is the substantial pressure build-up in the air gap between the upper part of the heat sink and the ceramic plaque. Additionally, the shape of the fins plays a significant role in temperature distribution. The rectangular fins effectively remove heat from the integrated inductor, resulting in a maximum temperature of 31.7°C. On the other hand, the square fins demonstrate efficient heat dissipation, leading to a maximum temperature of 33.8°C. The results will aid in the design and development of more efficient and reliable power converter systems, contributing to advancements in electronic device cooling and thermal management.

The correspondence address is:
Yamina BENHADDA,
Electrical Engineering Department,
USTO-MB University, Oran, Algeria.
Email: yamina.benhadda@univ-usto.dz

REFERENCES

[1] Derkaoui M., Benhadda Y., Chaabene G., Spiteri P., 32 (2023) Journal of Circuits, Systems, and Computers
[2] Benhadda, Y., Derkaoui, M., Mendaz, K., Kharbouch, H., & Spiteri, P., Periodica Polytechnica Electrical Engineering and Computer Science, 67 (2023), No. 4, 425–437
[3] Faraji H., Faraji M., El Alami M., IEEE, (2018)
[4] Bakhirathan A., Giridhar R., Gangadhara Kiran Kumar L., IEEE Transactions on components, packaging and manufacturing technology, 11 (2021), No. 8
[5] Seong-Ho S., Young-Se K., Electronic Components and Technology Conference, (2005).
[6] Sixel William R., Massoud K., Leary Alex M., AIAA Propulsion and Energy, (2021)
[7] Frommberger M., Schmutz C., Tewes M., McCord J., Wolfgang H., Reinhard L., Quandt E., IEEE Transactions on microwave theory and techniques, 53 (2005), No. 6
[8] Phillips Michael D., Raghu Kumar S., IEEE Transactions on microwave theory and techniques, 54 (2006), No. 4
[9] Jun-Yu O., Sen-Huei C., Huang-Ming L., Jong Ching W., IEEE TRANSACTIONS ON MAGNETICS, 45 (2009), No. 10